Supporting Information

Slime Mold-Bioinspired MXene Membrane for Efficient Uranium Immobilization

Yujie Shao, Yan Liu*, Zhirong Liu, Changfu Wang, Yun Wang, Dingzhong Yuan, Fengtao Yu, Ruiming Zhang, Hao Jiang*
National Key Laboratory of Uranium Resources Exploration-Mining and Nuclear Remote Sensing, East China University of Technology, Nanchang, Jiangxi 330013, PR China.

* Corresponding author: E-mail: fzliuyan1986@163.com; jianghaohpu@126.com

Experimental section

Materials

Titanium aluminum carbide (Ti_3AlC_2, MAX phase, 400 mesh) was purchased from Xinxi Technology Co., Ltd; lithium fluoride (LiF, AR grade), phytic acid (PA) sodium salt hydrate (≥ 90%), and ethylenediamine monohydrate (EDA, ≥ 98%) were obtained from Aladdin Reagent Co., Ltd; uranyl nitrate hexahydrate ($UO_2(NO_3)_2·6H_2O$, 99%), hydrochloric acid (HCl, 36-38%), and anhydrous ethanol were obtained from Sinopharm Chemical Reagent Co., Ltd. All chemicals were used as received without further purification.

Sample preparation

Preparation of $Ti_3C_2T_x$ suspension: A modified minimally intensive layer delamination method was employed. Briefly, 3.2 g of LiF was dissolved in 40 mL of 9 M HCl under stirring in a water bath at 40 °C for 15 min. Afterwards, 2 g of Ti_3AlC_2 powder was gradually added to the etchant and stirred for 24 h. The resulting black

slurry was washed repeatedly via centrifugation with 2 M HCl and deionized water (DIW) until the supernatant pH exceeded 5. The obtained multilayer $Ti_3C_2T_x$ sediment was then redispersed in DIW and subjected to ultrasonication in an ice bath under Ar atmosphere for 4 h. The final colloidal suspension of delaminated $Ti_3C_2T_x$ nanosheets was collected after centrifugation at 3500 rpm for 15-30 min to remove unexfoliated particles.

Preparation of composite membranes: A specified amount of EDA was added to a 12 mL of $Ti_3C_2T_x$ suspension (2.5 mg/mL) under stirring for 10 min. The mixture was transferred to a stainless-steel autoclave and heated to 70 °C for 6 h to obtain the amine-functionalized intermediate (denoted as ME). Following this, a corresponding amount of PA was added into the ME suspension and stirred for 30 min to obtain the phosphorylated composite (denoted as MEP). A control sample (MP) was fabricated by adding PA directly to the pristine $Ti_3C_2T_x$ suspension without EDA treatment. The free-standing membranes were produced by vacuum-assisted filtration of the respective suspensions and dried at 60 °C, assigned as MEP-1, MEP-2 and MEP-3, according to EDA : PA molar ratios of 1:1; 2:1; 1:2, respectively.

Characterization

Fourier transform infrared (FT-IR) spectra was recorded on a TENSOR27 spectrometer (Bruker) in transmission mode. Scanning electron microscopy (SEM) images and energy-dispersive X-ray spectroscopy (EDS) mapping were obtained using a JEOL JSM-5900LV microscope. X-ray photoelectron spectroscopy (XPS) analysis

was performed on a Kratos Axis Ultra DLD spectrometer with a monochromatic Al Kα X-ray source (1486.6 eV). All binding energies were calibrated relative to the adventitious C 1s peak at 284.8 eV. X-ray diffraction (XRD) patterns were collected on a Bruker D8 Advance diffractometer with Cu Kα radiation (λ = 1.5406 Å) at a scanning rate of 2°/min. Nitrogen adsorption-desorption isotherms were measured at 77 K using a V-Sorb 2800TP analyzer. Specific surface areas were calculated using the Bruauer-Emmett-Teller (BET) method, and pore size distributions were derived from the adsorption branch using the non-local density functional theory (NL-DFT) model. Electrochemical performance was carried out on a CHI660E electrochemical workstation (CH Instruments). Metal ion concentrations were determined by inductively coupled plasma mass spectrometry (ICP-MS, Agilent, 7850, USA).

Kinetic and Isotherm Models

The adsorption kinetics were analyzed using pseudo-first-order (PFO, Eq. S1) and pseudo-second-order (PSO, Eq. S2) models:

$$q_t = q_e(1 - e^{-k_1 t}) \tag{S1}$$

$$q_t = \frac{k_2 q_e^2 t}{1 + k_2 q_e t} \tag{S2}$$

where q_e and q_t (mg/g) are the adsorption capacities at equilibrium and at time t (min), respectively; k_1 (min^{-1}) and k_2 ($g \cdot mg^{-1} \cdot min^{-1}$) are the PFO and PSO rate constants.

The equilibrium adsorption data were fitted with Langmuir (Eq. S3) and Freundlich (Eq. S4) isotherm models:

$$q_e = \frac{q_m K_L C_e}{1 + K_L C_e} \quad \text{(S3)}$$

$$q_e = K_F C_e^{1/n} \quad \text{(S4)}$$

where C_e (mg/L) is the equilibrium concentration of U(VI); q_m (mg/g) is the theoretical maximum monolayer adsorption capacity; K_L (L/mg) is the Langmuir constant related to adsorption affinity; K_F (mg/g) and n are the Freundlich constants indicative of adsorption capacity and heterogeneity, respectively.

Electrochemical tests

Electrochemical impedance spectroscopy (EIS) was conducted in a three-electrode system using the membrane as the working electrode, a platinum foil as the counter electrode, and a $Hg/HgCl_2$ (saturated KCl) electrode as the reference electrode. The frequency range was 0.01 to 10^5 Hz with a 5 mV AC amplitude. Linear sweep voltammetry (LSV) was conducted in a three-electrode cell with an Ag/AgCl (3 M KCl) reference electrode and a Pt counter electrode. The electrolyte contained 200 ppm U(VI) and 0.5 M Na_2SO_4, as a supporting electrolyte, with a scan rate of 0.2 mv/s.

Batch adsorption experiments

All batch adsorption experiments were conducted at 298 K in a thermostatic shaker. The effects of pH (adjusted with 0.1 M HCl or NaOH), adsorbent dosage, contact time, and initial U(VI) concentration (20-400 mg/L) were investigated. The concentration of U(VI) in the supernatant was determined using the arsenazo(III) spectrophotometric method at a wavelength of 652 nm. The adsorption capacity q_t (mg/g) was calculated using Equation S5:

$$q_t = (C_0 - C_e)V/m \quad \text{(S5)}$$

where C_0 and C_e (mg/L) are the initial and equilibrium U(VI) concentrations, respectively, respectively; V (mL) is the solution volume; and m (mg) is the mass of the adsorbent.

Electrochemical Uranium Extraction

Electrochemical extraction tests were performed in a two-electrode batch cell with the MEP membrane (1 × 1 cm²) as the cathode and a Pt mesh as the anode. A square-wave potential was applied using a function/arbitrary waveform generator (DG1022Z, Rigol). The optimized waveform alternated between 0 V to -5 V with a frequency of 400 Hz and a duty radio of 50 % during the tests. All experiments were replicated three times.

DFT Computational Details

All density functional theory (DFT) calculations were carried out using the CP2K code [1]. All calculations employed a mixed Gaussian and planewave basis sets. Core electrons were represented with norm-conserving Goedecker-Teter-Hutter pseudopotentials [2-4], and the valence electron wavefunction was expanded in a double-zeta basis set with polarization functions [5] along with an auxiliary plane wave basis set with an energy cutoff of 450 Ry. The generalized gradient approximation exchange-correlation functional of Perdew, Burke, and Enzerhof (PBE) [6] was used. Each configuration was optimized with the Broyden-Fletcher-Goldfarb-Shanno (BGFS) algorithm with SCF convergence criteria of 1.0×10^{-5} au. To compensate the

long-range van der Waals dispersion interaction, the DFT-D3 scheme [7] with an empirical damped potential term was added into the energies obtained from exchange-correlation functional in all calculations.

The interaction energy between the adsorbate and the substrate can be calculated as:

$$\Delta E_{ads} = E_{adsorbate@substrate} + E_{substrate} - E_{adsorbate} \quad \text{(S6)}$$

where $E_{adsorbate@substrate}$ and $E_{substrate}$ represent the total energies of the substrate with and without the adsorption of adsorbate, respectively. $E_{adsorbate}$ is the total energy of the adsorbate UO_2^{2+}. According to this equation, a negative adsorption energy corresponds to a stable adsorption structure.

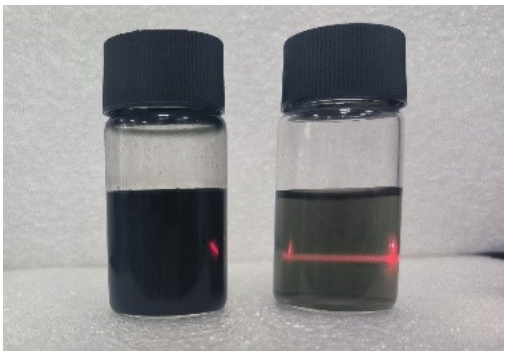

Fig. S1 Tyndall effect observed in a colloidal solution of delaminated $Ti_3C_2T_x$.

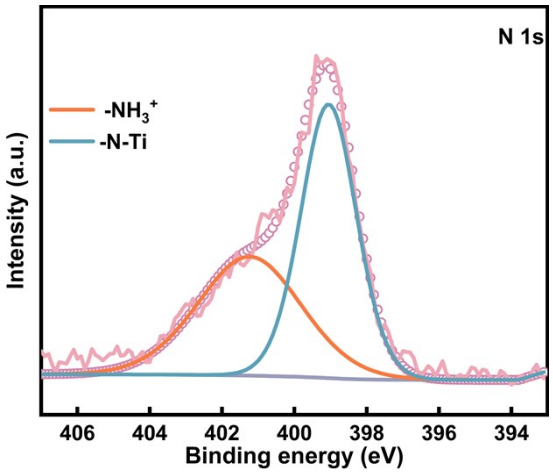

Fig. S2 High-resolution N 1s XPS spectra of the MEP membrane.

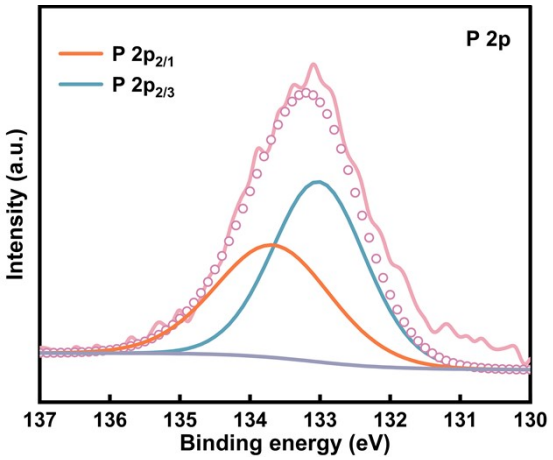

Fig. S3 High-resolution P 2p XPS spectra of the MEP membrane.

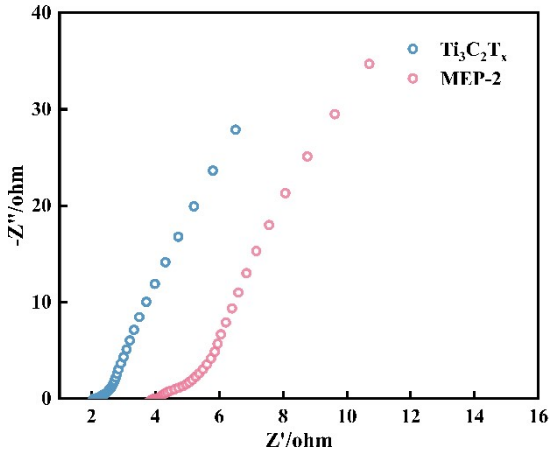

Fig. S4 Nyquist plots for pristine $Ti_3C_2T_x$ and the MEP-2 membrane.

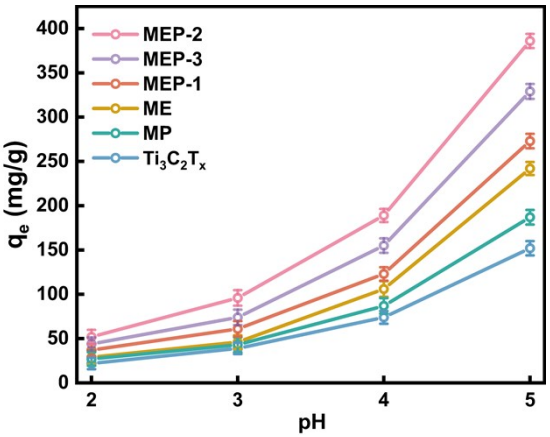

Fig. S5 The influence of different EDA : PA molar ratios and pH on U(VI) adsorption capacity.

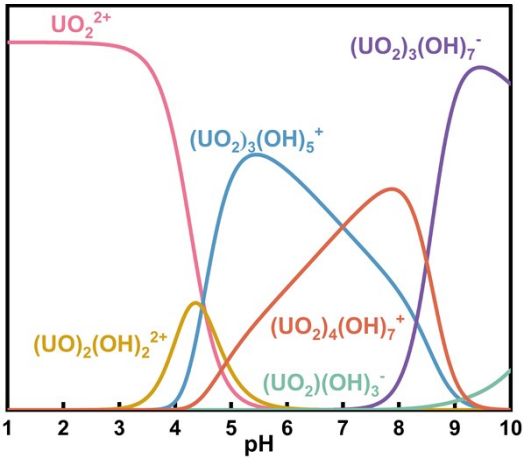

Fig. S6 Distribution of uranium morphologies at different pH.

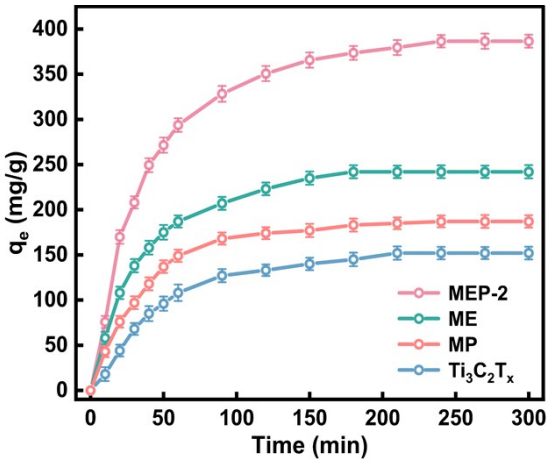

Fig. S7 Effect of time on adsorption performance.

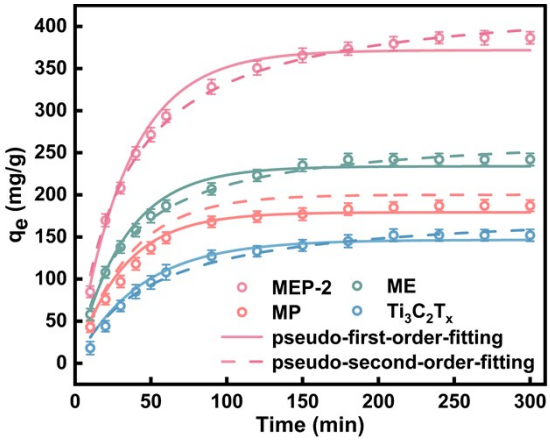

Fig. S8 Kinetics fitting plots.

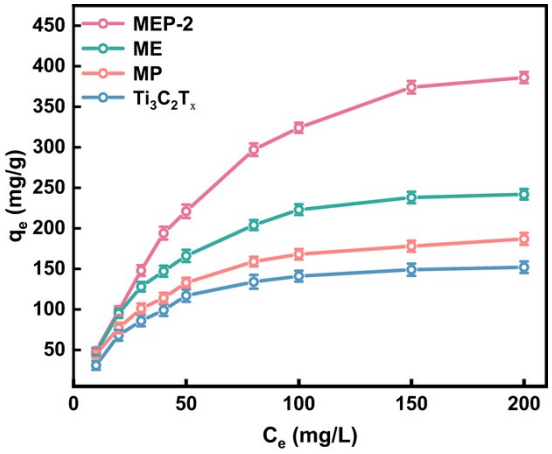

Fig. S9 Effect of initial concentrations on adsorption performance.

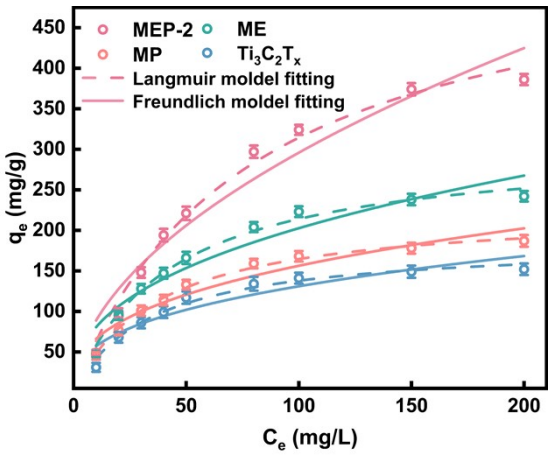

Fig. S10 Eequilibrium isotherms fitting for U(VI) adsorption on MEP-2.

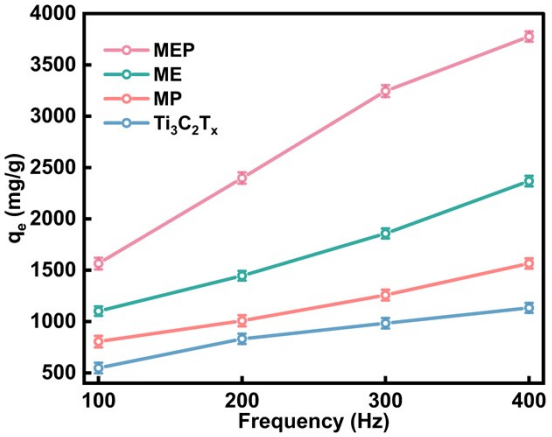

Fig. S11 Effect of applied frequency on U(VI) extraction capacity.

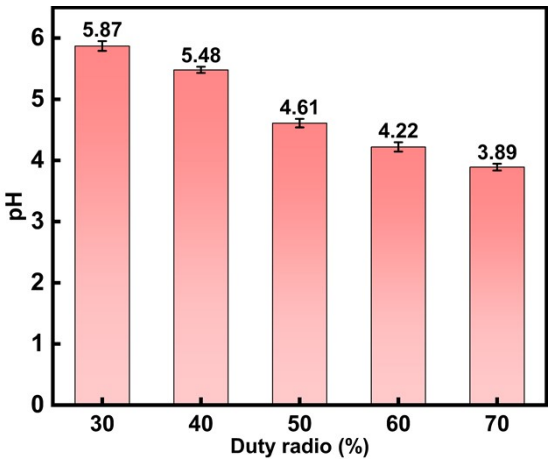

Fig. S12 The variance of pH values at different duty radios of MEP-2.

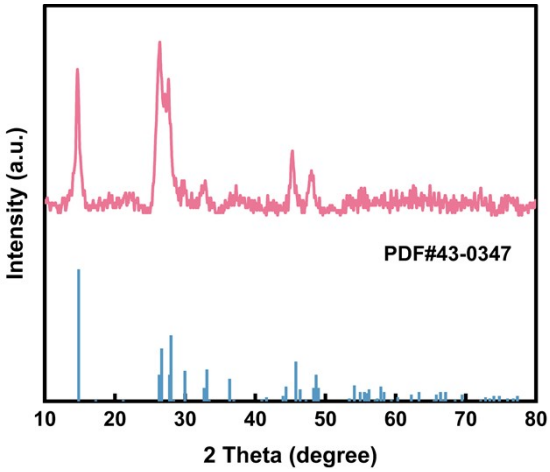

Fig. S13 XRD pattern of the electrochemically generated deposits.

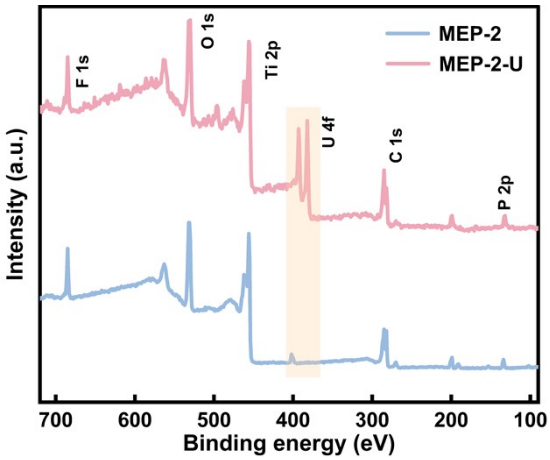

Fig. S14 XPS full spectra of MEP-2 and MEP-2-U.

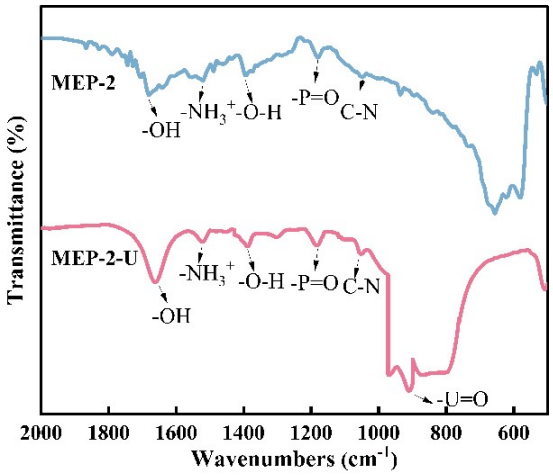

Fig. S15 FT-IR spectra of the MEP-2 membrane before and after electro-extraction.

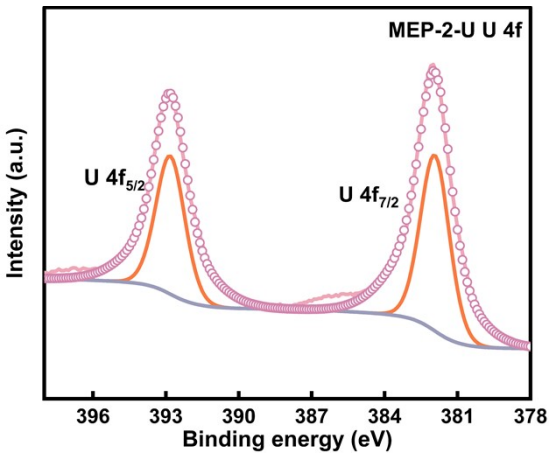

Fig. S16 High-resolution U 4f spectrum of MEP-2-U.

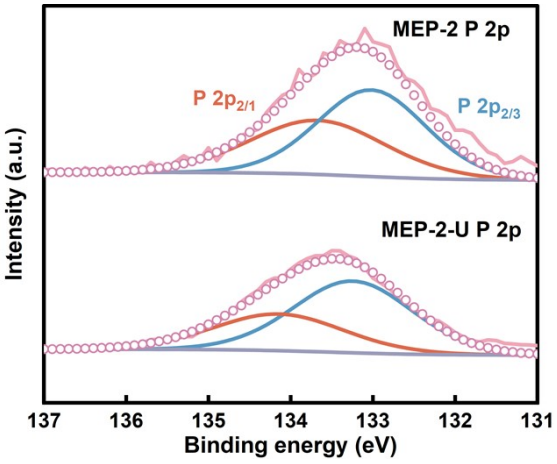

Fig. S17 High-resolution P 2p XPS spectra of the MEP-2 membrane before and after uranium extraction.

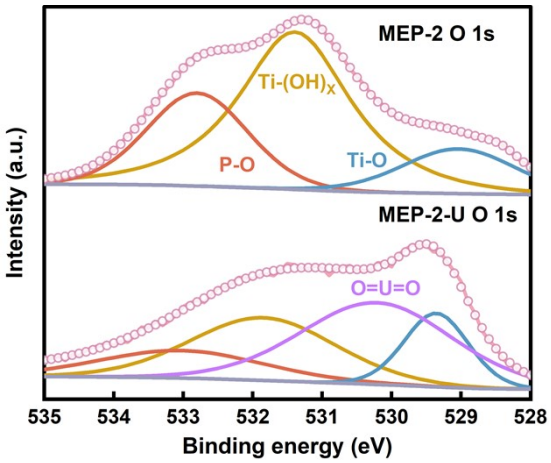

Fig. S18 High-resolution O 1s XPS spectra of the MEP-2 membrane before and after uranium extraction.

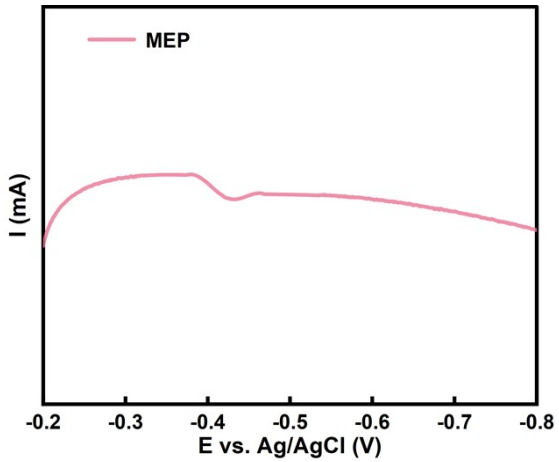

Fig. S19 LSV curve of the MEP-2 electrode in uranium-spiked aqueous solution.

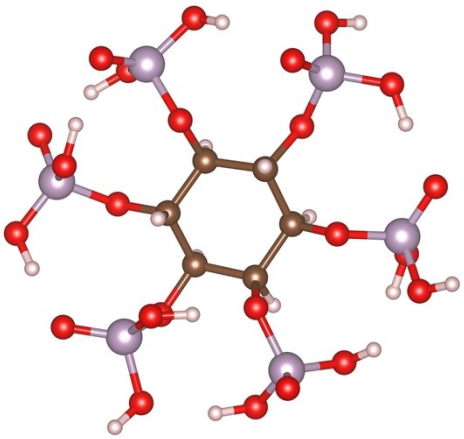

Fig. S20 DFT-optimized molecular structure of PA.

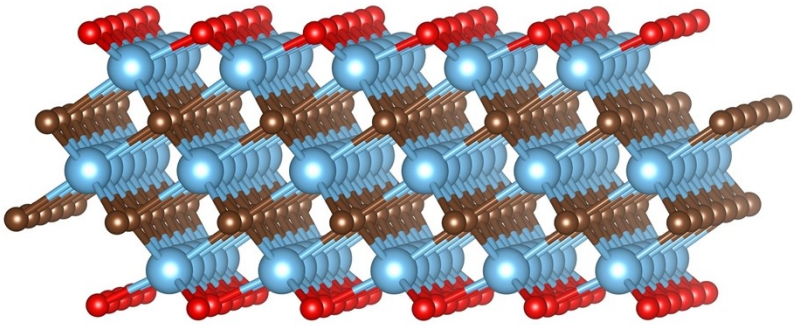

Fig. S21 DFT-optimized structure of a $Ti_3C_2O_2$ MXene monolayer model used in the calculations.

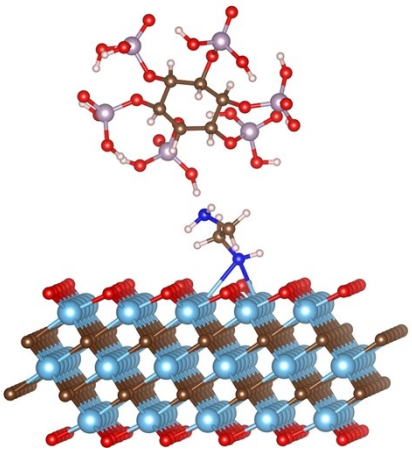

Fig. S22 DFT-optimized structural model of the MEP composite.

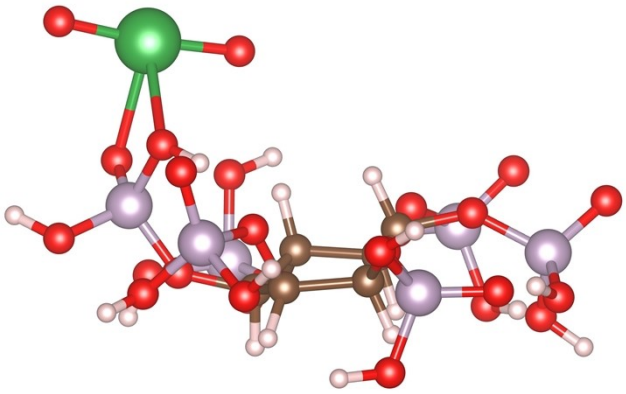

Fig. S23 DFT-optimized adsorption configuration of a UO_2^{2+} ion on a PA molecule.

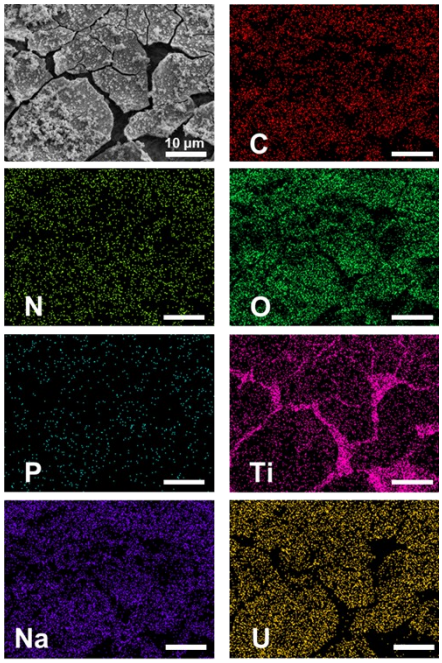

Fig. S24 SEM and EDS image of MEP-2 after electrochemical extraction.

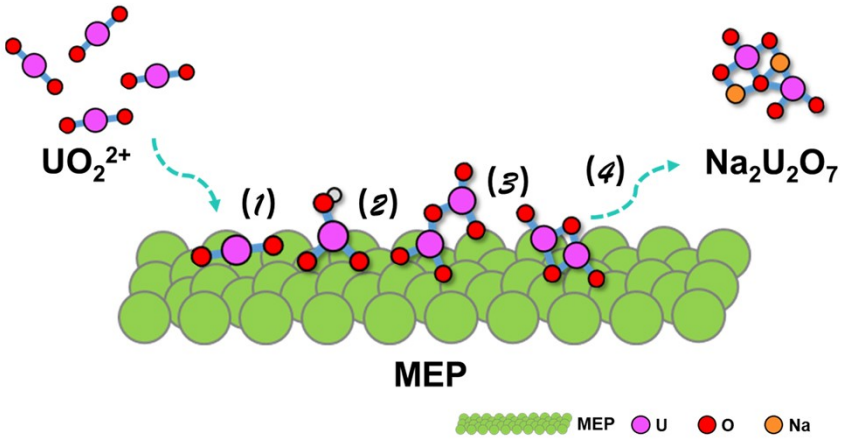

Fig. S25 Schematic diagram of the proposed conversion mechanism of uranyl ions on the MEP electrode.

Table S1 Kinetic parameters derived from PFO and PSO models for U(VI) by $Ti_3C_2T_x$, ME, MP, MEP-2.

Sample	$q_{e,exp}$ (mg/g)	Pseudo-first-order model			Pseudo-second-order model		
		$q_{1,cal}$ (mg/g)	k_1 (min^{-1})	R^2	$q_{2,cal}$ (mg/g)	k_2 (min^{-1})	R^2
$Ti_3C_2T_x$	152	146.53	2.33×10-2	0.9796	184.36	1.11×10-4	0.9821
ME	242	233.89	3.11×10-2	0.9771	276.35	1.18×10-4	0.9889
MP	207	200.11	2.90×10-2	0.9781	240.78	1.27×10-4	0.9900
MEP-2	386	371.83	2.71×10-2	0.9854	437.95	7.03×10-5	0.9940

Table S2 Isotherm parameters determined by Langmuir and Freundlich model fitting for U(VI) adsorption onto $Ti_3C_2T_x$, ME, MP, MEP-2.

Sample	Langmuir			Freundlich		
	q_m(mg/g)	K_L(L/mg)	R^2	K_F (mg/g)(L/mg)$^{1/n}$)	n	R^2
$Ti_3C_2T_x$	560.66	0.013	0.9902	26.69	2.14	0.9450
ME	305.25	0.024	0.9910	32.01	2.49	0.9215
MP	254.93	0.027	0.9979	27.10	2.51	0.9450
MEP-2	185.10	0.029	0.9825	24.79	2.77	0.8893

Table S3. Comparison of the maximum U(VI) adsorption capacity of the MEP-2 membrane with other previous literature.

Sample	Equilibrium time	pH	Adsorption capacity (mg/g)	Refs.
V_2CT_x MXene	4.5 h	5.0	174.0	[8]
Hydrated $Ti_3C_2T_x$	360 min	5.0	214.0	[9]
porous MXene	180 min	5.0	299.0	[10]
TCCH	3 min	5.0	344.8	[11]
MXene/PAO	24 h	5.0	356.0	[12]
GO/HAP	5 min	3.0	373.0	[13]
GOS	180 min	6.0	309.9	[14]
COF-HBI	30 min	4.5	211.0	[15]
Fe_3O_4@Ti_3C_2-PDA/OA	3 h	5.0	165.9	[16]
MEP-2	**180 min**	**5.0**	**368**	**This work**

Table S4. Comparison of the maximum U(VI) electrochemical adsorption capacity of the MEP-2 membrane with previous literature.

Sample	Equilibrium time	Adsorption capacity (mg/g)	Refs.
$Na_3MnTi(PO_4)_3$@C	5 h	499.69	[17]
UiO-66-CN	5 h	3052.00	[18]
T_1V_1	12 h	1852.00	[19]
TCP-2	12 h	2809.00	[20]
C-Ami	12 h	1932.00	[21]
TFPM-PDAN-AO	12 h	4685.00	[22]
MEP-2	**10 h**	**3776.25**	**This work**

References

[1] J. VandeVondele, M. Krack, F. Mohamed, M. Parrinello, T. Chassaing, J. Hutter, Quickstep: Fast and accurate density functional calculations using a mixed Gaussian and plane waves approach. Comput. Phys. Commun., 167 (2005) 103-128.

[2] S. Goedecker, M. Teter, J. Hutter, Separable Dual-Space Gaussian Pseudopotentials. Phys. Rev. B, 54 (1996) 1703-1710.

[3] C. Hartwigsen, S. Goedecker, J. Hutter, Relativistic Separable Dual-Space Gaussian Pseudopotentials from H to Rn. Phys. Rev. B, 58 (1998) 3641-3662.

[4] M. Krack, M. Parrinello, All-electron ab-initio Molecular Dynamics. Phys. Chem. Chem. Phys., 2 (2000) 2105-2112.

[5] J. VandeVondele, J. Hutter, Gaussian Basis Sets for Accurate Calculations on Molecular Systems in Gas and Condensed Phases. J. Chem. Phys., 127 (2007) 114105.

[6] J. P. Perdew, K. Burke, M.Ernzerhof, Generalized gradient approximation made simple. Phys. Rev. Lett., 77 (1996) 3865.

[7] S. Grimme, J. Antony, S. Ehrlich, H. Krieg, A Consistent and Accurate ab initio Parametrization of Density Functional Dispersion Correction (DFT-D) for the 94 Elements H-Pu. J. Chem. Phys., 132 (2010) 154104.

[8] L. Wang, L. Yuan, K. Chen, Y. Zhang, Q. Deng, S. Du, Q. Huang, L. Zheng, J. Zhang, Z. Chai, M.W. Barsoum, X. Wang, W. Shi, Loading Actinides in Multilayered Structures for Nuclear Waste Treatment: The First Case Study of Uranium Capture with Vanadium Carbide MXene, ACS Appl. Mater. Interfaces, 8 (2016) 16396–16403.

[9] L. Wang, W. Tao, L. Yuan, Z. Liu, Q. Huang, Z. Chai, J.K. Gibson, W. Shi, Rational control of the interlayer space inside two-dimensional titanium carbides for highly efficient uranium removal and imprisonment, Chem. Commun., 53 (2017) 12084–12087.

[10] Y. Wang, Z. Lu, M. Luo, Z. Zhao, Y. Wei, H. Wang, Enhanced uranium adsorption performance of porous MXene nanosheets, Sep. Purif. Technol., 335 (2024) 126134.

[11] P. Zhang, L. Wang, K. Du, S. Wang, Z. Huang, L. Yuan, Z. Li, H. Wang, L. Zheng, Z. Chai, W. Shi, Effective removal of U(VI) and Eu(III) by carboxyl functionalized MXene nanosheets, J. Hazard. Mater., 396 (2020) 122731.

[12] Y. Zhou, J. Yang, N. Zhou, H. Hao, X. Jiang, F. Lei, K. Shi, Y. Zhao, G. Zhou, T. Liu, S. Xing, Amidoxime-Functionalized MXene beads for the effective capture of uranium from wastewater with high fluoride concentrations, Chem. Eng. J., 471 (2023) 144647.

[13] M. Su, Z. Liu, Y. Wu, H. Peng, T. Ou, S. Huang, G. Song, L. Kong, N. Chen, D. Chen, Graphene oxide functionalized with nano hydroxyapatite for the efficient removal of U(VI) from aqueous solution, Environ. Pollut., 268 (2021) 115786.

[14] Z. Zhang, Y. Qiu, Y. Dai, P. Wang, B. Gao, Z. Dong, X. Cao, Y. Liu, Z. Le,

Synthesis and application of sulfonated graphene oxide for the adsorption of uranium(VI) from aqueous solutions, J. Radioanal. Nucl. Chem., 310 (2016) 547–557.
[15] J. Li, X. Yang, C. Bai, Y. Tian, B. Li, S. Zhang, X. Yang, S. Ding, C. Xia, X. Tan, L. Ma, S. Li, A novel benzimidazole-functionalized 2-D COF material: Synthesis and application as a selective solid-phase extractant for separation of uranium, J. Colloid Interface Sci., 437 (2015) 211–218.
[16] F. Liu, Z. Hu, M. Xiang, B. Hu, Magnetic amidoxime-functionalized MXenes for efficient adsorption and immobilization of U(VI) and Th(IV) from aqueous solution, Appl. Surf. Sci., 601 (2022) 154227.
[17] Y. Chen, X. Yin, N. Zheng, Z. Lin, T. Fujita, S. Ning, Y. Chen, X Wang, Flexible self-supporting $Na_3MnTi(PO_4)_3$@C fibers for uranium extraction from seawater by electro sorption, J. Hazard. Mater., 461 (2024) 132664.
[18] J. Tian, N. Li, Y. Luo, H. Xing, R. Su, L. Wang, Construction of a graphene/cellulose aerogel embedded with UiO-66-CN for highly efficient uranium capture via electro-adsorption, J. Mater. Chem. A, 13 (2025) 6597-6606.
[19] H. Chen, Y. Shao, Y. Liu, Z. Liu, C. Wang, W. Liu, F. Yu, Y. Wang, D. Yuan, H. Jiang, Electro-trapping uranium with a cost-effective and scalable ice-templated MXene/VMT electrode, Chem. Commun., 61 (2025) 18898-18901.
[20] R. Zhang, J. Liu, Z. Liu, X. Duan, F. Yu, Y. Wang, D. Yuan, H. Jiang, Y. Liu, Flexible self-standing amidoxime-functionalized MXene membrane for electrochemical uranium extraction, J Colloid Interface Sci., 679 (2025) 547-554.
[21] C. Liu, P. Hsu, J. Xie, J. Zhao, T. Wu, H. Wang, W. Liu, J. Zhang, S. Chu, Y. Cui. A half-wave rectified alternating current electrochemical method for uranium extraction from seawater. Nat. Energy, 2 (2017) 17007.
[22] C. Zhang, J. Qi, W. Cu, X. Chen, X. Liu, S. Yi, C. Niu, R. Liang, J. Qiu. A novel 3D sp^2 carbon-linked covalent organic framework as a platform for efficient electro-extraction of uranium. Sci. China Chem., 66 (2022) 562-569.